Synthesis and properties of allylic, benzylic, propargylic and allenylic oxonium ions

Hau Sun Sam Chan,[1] Yingzi Li,[2] Jack L. Sutro,[1] Daniel Brown,[1] Robert S. Paton,[2]* and Jonathan W. Burton[1]*

[1] Chemistry Research Laboratory, Department of Chemistry, University of Oxford, 12 Mansfield Road, Oxford, OX1 3TA, UK.
[2] Department of Chemistry, Colorado State University, 1301 Center Ave, Ft. Collins, CO 80523-1872, USA.

E-mail: robert.paton@colostate.edu; homepage: https://patonlab.com
jonathan.burton@chem.ox.ac.uk; homepage: http://burton.web.ox.ac.uk

Abstract: Despite numerous studies of trialkyloxonium ions in the literature, investigations into the chemistry of allylic, benzylic, propargylic and allenylic oxonium ions are rare. Existing reports on well-characterised allylic and benzylic oxonium ions invariably construct these species based on constrained tricyclic oxatriquinane/oxatriquinacene scaffolds, with only limited studies reported on unconstrained benzylic oxonium ions. Herein we report an investigation on a collection of allylic, benzylic and hitherto unknown propargylic and allenylic oxonium ions prepared on unconstrained scaffolds by a general, modular and unified strategy. Permutation of the substitution pattern of these oxonium ions allowed the extension of the strategy for the syntheses of various doubly-substituted oxonium ions. Most of these oxonium ions could be characterised at room temperature by NMR, and a series of unexpected reactions and chemical behaviour pertinent to these species are briefly described.

Introduction

The first trialkyloxonium ion $Me_3O^+BF_4^-$ **1** was reported by Meerwein and co-workers in 1937.[1] Over the years, increasingly sophisticated members of this class of compound have been disclosed. Selected examples include: substituted tetrahydrofuranyl and bicyclic oxonium ions **2**, **3** by Gargiulo and Tarbell,[2] three to five membered cyclic oxonium ions **4**-**6** by Lambert and Johnson,[3] and six membered cyclic oxonium ions **7** by Klages, Gordon and Jung.[4] Meerwein and co-workers have also reported the synthesis of the oxonium ions **6** and **7**.[5] The *C*-silylated oxonium ion **8** and 1-oxoniaadamantane **9** were reported by Olah and co-workers,[6,7] 1-oxoniabicyclo[2.2.2]octane **10** by Klages, Jung and Wagner,[8] and the bisoxonium ion **11** by Smith, Schultz and Newmark.[9] More recently, a series of oxatriquinanes **12**–**14** and their functionalised analogues were prepared by Mascal and co-workers,[10-13] and also by Suzuki and Muratake.[14] The latest addition to the series was a family of biosynthetically relevant trialkyloxonium ions **15** and **16** from our own group (**Figure 1a**).[15] The corresponding triaryloxonium ions, which are considerably more stable than trialkyloxonium ions, were first reported in 1957 with the synthesis of triphenyloxonium tetrafluoroborate **19**[16, 17] and have recently been exploited by us[18] and others[19] as mild precursors (**20**) for the synthesis of *o*-arynes[20, 21] and in the synthesis of a helically chiral oxonium ion bearing a stereogenic oxygen atom **21**.[22]

Trialkyl oxonium ions bearing allylic, benzylic, propargylic and allenylic substituents are rare with only five well-characterized examples **14e**, **14j**, **14n**, **17** and **18** having allylic or benzylic substituents prepared on constrained oxatriquinane and oxatriquinacene skeletons that confer unusual stability on these species.[10, 14] Oxatriquinacene **18** was reported as a triply bis-allylic oxonium ion, however, the constrained nature of its scaffold precludes considerable overlap between the vacant $\sigma^*_{C-O^+}$ orbitals with the $\pi_{C=C}$ orbitals of the olefins; thus the constitutionally allylic positions are not necessarily stereoelectronically allylic.[23-25] Although both benzylic and allylic oxonium ions have been proposed as reaction intermediates,[26-30] literature reports of such oxonium ions on unconstrained scaffolds are limited and lack extensive characterisation (see Supplementary Information page S2 for examples).[31-33] For example, the benzylic oxonium ion **22** reported by Olah, was formed at –90 °C in SbF_5-SO_2ClF solution and characterised by ^{1}H NMR, and was found to be highly thermally unstable, decomposing into anisole and polymeric material above −70 °C.[33] Herein we report the preparation and description of the behaviour of a series of unconstrained allylic, benzylic, and hitherto unknown propargylic and allenylic oxonium ions as evidenced by comprehensive NMR spectroscopic characterization supported by DFT calculations, with the aim of elucidating the chemistry of these species without the constraints imparted by the oxatriquinane and oxatriquinacene skeletons (**Figure 1b**).

Results and discussion

Synthesis and characterization of the oxonium ions

Our strategy for the preparation of the various unsaturated oxonium ions builds on our previous work[15, 34] and was to promote substitution of a halide leaving group by an ether oxygen atom using a silver(I) salt that has a non-nucleophilic counter anion. In practice, the oxonium ions **24** were synthesized by halide abstraction from the corresponding bromides or chlorides **23** (see Supplementary Information, page S5 and from page S6 onwards for detailed procedures for the preparation of the cyclisation substrates) by mixing with $AgSbF_6$ or $AgAl(pftb)_4{\cdot}CH_2Cl_2$ [pftb = tetrakis(perfluoro-*tert*-butoxy)aluminate][35] in CD_2Cl_2 in a J. Young NMR tube and allowing the precipitated silver(I) halide to settle before acquisition of NMR data (**Figure 2b**). The temperatures at which halide abstraction was performed for the generation of the oxonium ions were identical to that of their NMR acquisition temperatures unless otherwise specified (**Figure 2c-e**). Using this methodology, we prepared [3.3.0] and [4.3.0]-bicyclic benzylic, allylic, propargylic and allenylic oxonium ions carrying substituents ranging from phenyl, vinyl and ethynyl groups to enoates, enynes and carboxy allenes. All of these oxonium ions were readily formed as the major species which were subsequently characterised by NMR spectroscopy between –20 and +20 °C.

Characterization of the oxonium ions began with analysis of the NMR spectroscopic data of the monosubstituted series **24a**•SbF_6 and **24b–24j**•$Al(pftb)_4$ (**Figure 2c-e**). The protons attached to the carbon atoms adjacent to the trivalent oxygen (the α-protons), resonate within the range of 4.0–5.9 ppm in the corresponding ^{1}H NMR spectra, with the methylene protons generally resonating at lower chemical shift compared with the methine protons, in keeping with literature data (**Figure 2a**).[7, 10, 14] In the ^{13}C NMR spectra the oxonium ion α-carbons resonate in the range of 79.7–108.0 ppm, and follow the same trend. Evidence to support the trivalency of the oxonium ion oxygen atom in these

species was provided by ^{1}H-^{13}C HMBC correlations between the oxonium ion α-protons and α-carbons. Using oxonium ion **24c**•Al(pftb)$_4$ as an example (**Figure 2c**), ^{1}H-^{13}C HMBC correlations were observed between the blue protons and the green and orange carbons simultaneously, which is only possible if the oxonium ion oxygen is trivalent (see Supplementary Data, pages 125–267 for the NMR spectra of all the reported oxonium ions). The same pattern was also observed for oxonium ion **24f**•Al(pftb)$_4$ (**Figure 2d**). For oxonium ions such as (*Z*)-**24h**•Al(pftb)$_4$ (**Figure 2e**) in which its ^{1}H-^{13}C HMBC correlations were too weak to be observed (see Supplementary Data, page 172), trivalency was inferred by analogy with the closely related oxonium ions reported herein. With all the oxonium ions reported in this study, the oxygen atom is a stereogenic centre; however, given that the barrier to pyramidal inversion at oxygen in trialkyloxonium ions is less than 10 kcal/mol,[3] we sought to determine whether *cis* or *trans* ring fusion was favoured for the oxonium ions shown in **Figure 2** using DFT calculations and, where appropriate, ^{1}H NMR nOe experiments. DFT calculations on the pare **24a**, **24b**, and **24c** (anion excluded) indicated that the *trans*-fused [3.3.0]-bicyclic oxonium ions are not energy minima: on geometry optimisation they spontaneously undergo inversion at oxygen to yield the *cis*-fused [3.3.0]-bicyclic structures (see Supplementary Information pages S90–S91). On this basis, the [3.3.0]-bicyclic oxonium ions were assigned with a *cis* ring fusion. The overall relative configurations of the *cis*-fused [3.3.0]-bicyclic oxonium ions were established by comparison of their ^{1}H and ^{13}C NMR chemical shifts to those simulated by DFT calculations for the two possible *cis*-fused [3.3.0]-bicyclic diastereomers, as the observed ^{1}H NMR NOESY correlations of these oxonium ions did not allow unambiguous assignment of relative configuration (see Supplementary Information pages S94–S104). The ring fusion of the [4.3.0]-bicyclic oxonium ions was assigned as *trans* on the basis of DFT calculations and ^{1}H NMR nOe experiments. DFT calculations indicated that for the [4.3.0]-bicyclic oxonium ions the *trans*-fused diastereomeric conformer is universally lower in energy than the *cis*-fused one (1.4–1.9 kcal/mol) as in the parent hydrindane below 200 °C (see Supplementary Information S90-S92).[36] Again the relative configurations of the [4.3.0]-bicyclic oxonium ions were assigned by comparison of their ^{1}H and ^{13}C NMR chemical shifts to those simulated by DFT calculations for the two possible *trans*-fused [4.3.0]-bicyclic oxonium ion diastereomers (see Supplementary Information pages S105–S108); for oxonium ion **24f**•Al(pftb)$_4$ the assignment of the relative configuration was supported by ^{1}H NMR nOe analysis (see Supplementary Data page 155).

A host of oxonium ions bearing adjacent unsaturation at two positions **24k–24v**•Al(pftb)$_4$ (**Figure 3**) were also readily prepared through silver-mediated halide abstraction from the corresponding monocyclic precursors. As with the oxonium ions **24a**•SbF_6 and **24b–24j**•Al(pftb)$_4$, the oxonium ions **24k–24v**•Al(pftb)$_4$ were formed as the major solution species on treatment of the corresponding alkyl halide with AgAl(pftb)$_4$·CH_2Cl_2. With these oxonium ions, the oxonium ion α-protons resonate within the range of 4.4–5.9 ppm and the oxonium ion α-carbons resonate in the range of 80.8–125.4 ppm in their ^{1}H and ^{13}C NMR spectra respectively, largely in keeping with the monosubstituted series. Evidence to support the trivalency of the oxonium ion oxygen was again provided by ^{1}H-^{13}C HMBC correlations between the oxonium α-protons and α-carbons. Using oxonium ion **24r**•Al(pftb)$_4$ as an

example, ^{1}H-^{13}C HMBC correlations were observed between the blue protons and the green and red carbons simultaneously, which is only possible if the oxonium ion oxygen is trivalent. In addition, the ^{1}H-^{13}C HMBC correlation between the green proton and the blue carbon was also observed. The same pattern of correlation was also found for oxonium ion **24p**•Al(pftb)$_4$ (**Figure 3a–b**, see Supplementary Data for other disubstituted oxonium ions). Species with weak ^{1}H-^{13}C HMBC correlations, such as **24v'**•Al(pftb)$_4$, were characterised by analogy with closely related oxonium ions. The relative configurations of several members of the disubstituted oxonium ions **24l**•Al(pftb)$_4$, **24m**•Al(pftb)$_4$, **24n**•Al(pftb)$_4$, **24p**•Al(pftb)$_4$, **24q**•Al(pftb)$_4$ and **24r**•Al(pftb)$_4$ were elucidated by ^{1}H-^{1}H NOESY correlations, with the relative configurations of the remaining members assigned by analogy. Disubstitution of the oxonium ions enabled further expansion of the scope of the oxonium ions, rendering the synthesis of enal oxonium ions **24q**•Al(pftb)$_4$ and *p*-methoxybenzyl oxonium ions **24p**•Al(pftb)$_4$ and **24v**•Al(pftb)$_4$ possible. The syntheses of the corresponding monosubstituted enal and *p*-methoxybenzyl oxonium ions were plagued by poor solubility of the enal oxonium ion, and poor stability of the halide precursor of *p*-methoxybenzyl oxonium ion.

Properties of the oxonium ions: Stereochemical behaviour

The oxonium ions **24** were formed from diastereomeric mixtures of halides **23**. However, NMR analysis of the twenty-two synthesised oxonium ions (**Figure 2** and **Figure 3**), showed that thirteen of the oxonium ions were predominantly single diastereomers. This observation may result from an oxonium ion-carbenium ion equilibrium,[12] in which the C–O$^+$ bonds of the oxonium ions **24** would be labile and thus allow conversion of one diastereomer into another. Alternatively, selective decomposition of one diastereomer into NMR-silent species (e.g. by polymerization and precipitation) would also be in keeping with predominantly single diastereomers being observed. To distinguish these two possibilities, the oxonium ions **24m**•SbF_6 and **24m'**•SbF_6 were generated with $AgSbF_6$ at −20 °C and were characterized as a 2.2 : 1 diastereomeric mixture by ^{1}H NMR at –20 °C followed by incubation of the NMR sample in the spectrometer at 0 °C which lead to equilibration into a single diastereomer over 30 minutes (**Figure 4**). Quantitative NMR (QUANTAS)[37] experiments indicated that selective decomposition of one diastereomer of **24m/24m'**•SbF_6 was not occurring but rather that **24m'**•SbF_6 was being converted into **24m**•SbF_6 most likely *via* an oxonium ion-carbenium ion equilibrium. This was evident from the observation that the total integral of the highlighted methylene protons of **24m**•SbF_6 (purple) and **24m'**•SbF_6 (orange) remained constant over 30 minutes, and the decay of the integral of **24m'**•SbF_6 was accompanied by the simultaneous growth of the integral of **24m**•SbF_6 (**Figure 4b**). Three plausible pathways for the oxonium ion-carbenium ion equilibrium of oxonium ions **24** by heterolysis of C–O$^+$ bonds are shown in **Figure 4c** two of which, pathways b and c, can lead to stereochemical inversion. From the reported literature values of gas phase hydride affinity of carbenium ions (**Figure 4d**),[38-40] C–O$^+$ bond heterolysis by pathway *c* is predicted to be the most likely (most stable tertiary carbenium ion) for the interconversion of doubly substituted oxonium ions, followed by pathway *b*. DFT calculations indicated that formation of an allylic carbenium ion, pathway *b*, is reasonable with a barrier of 21–22 kcal/mol for **24m** (19–21 kcal/mol for **24m'**), which compares favourably with the measured barrier (19.3 kcal/mol, see Supplementary

Information pages S86 and S109). For pathway *c* with **24m**, the benzylic carbenium ion is calculated to be the most stable intermediate; however, the barrier for ring opening to give the benzylic carbenium ion **27m** is higher than to form the allylic carbenium ion **26m** hence for oxonium ions **24m/24m'**•SbF_6 equilibration most likely proceeds *via* pathway *b*. For the monosubstituted oxonium ions (**Figure 2**) it is likely that the interconversion of the diastereomeric oxonium ions occurs *via* pathway *b* as pathway *c* would result in a higher energy secondary carbenium ion; DFT calculations indicated that formation of a primary carbenium ion **25** is energetically extremely unfavourable and unavailable for all of oxonium ions **24**.

An extreme case of equilibration of diastereomeric oxonium ions is illustrated by the *p*-methoxybenzylpropargyl oxonium ion **24v/24v'**•Al(pftb)$_4$. With a highly cation stabilising substituent (*p*-methoxyphenyl, Hammett substituent constant $\sigma = -0.27$)[41] at the transannular (red) position, this oxonium ion was found to be fluxional by NMR even at −40 °C (**Figure 5a-c**) as evidenced by the presence of exchange cross-peaks (red off-diagonal peaks; blue off-diagonal peaks are nOe's) in the ^{1}H NMR NOESY spectrum of **24v/24v'**•Al(pftb)$_4$. The proton resonances of the blue and green protons on the oxonium ion scaffold of **24v/24v'**•Al(pftb)$_4$, the purple and magenta protons on the aromatic ring, and the grey acetylenic proton of the two diastereomers were undergoing exchange. By comparison the benzylpropargyl oxonium ion **24s**/**24s'**•Al(pftb)$_4$ which has a less electron donating phenyl group ($\sigma = 0$), did not appear fluxional by NMR even at 0 °C, as shown by the absence of exchange cross-peaks of the corresponding blue, green, purple, magenta and grey protons in the ^{1}H NMR NOESY spectrum (**Figure 5d**). Considering the gas phase hydride affinities of the incipient carbenium ions, it is unlikely for an oxonium ion-carbenium in equilibrium to be established through pathway *b* in **24v/24v'**•Al(pftb)$_4$ as the incipient secondary propargyl carbenium is expected to be significantly higher in energy compared with the tertiary *p*-methoxybenzyl carbenium ion. Therefore, the fluxionality observed likely arises through pathway *c* between the oxonium ion pairs **24v**/*ent*-**24v'**•Al(pftb)$_4$ and *ent*-**24v**/**24v'**•Al(pftb)$_4$, with **27v**/*ent*-**27v**•Al(pftb)$_4$ as proposed intermediates. This proposal was supported by DFT calculations with the barrier to *p*-methoxybenzyl carbenium ion formation calculated to be 16-17 kcal/mol (see Supplementary Information page S110). Furthermore, the benzylic system **24s**/**24s'**•Al(pftb)$_4$ was not found to be fluxional by NMR at 0 °C despite possessing the same secondary propargyl carbenium ion intermediate if pathway *b* were operative. The observed diastereomeric ratio of the oxonium ions **24v**/**24v'**•Al(pftb)$_4$ (1.7-1.8:1, at −40 °C) reflects the relative thermodynamic stability of the two diastereomers. The variation in line shape of the ^{1}H NMR resonances for **24v**/***ent*-24v'**•Al(pftb)$_4$ with respect to changing temperature is due to chemical exchange not decomposition, as evidenced by the reversible behaviour of the ^{1}H NMR resonances between 246K (−27 °C) and 298K (25 °C) (**Figure 5b**).

The proposed *O*-methylated *p*-quinone methide cations **27v**/*ent*-**27v**•Al(pftb)$_4$ could be trapped with a series of nucleophiles to provide oxocanes **28**-**33**. Initially we found the trapping reactions of **27v**/*ent*-**27v**•Al(pftb)$_4$ by nucleophiles such as furans, allylsilanes and silyl ketene acetals to be highly

irreproducible. We attributed the capricious nature of these quenching reactions to the formation of Brønsted or Lewis acidic cations under the reaction conditions which decomposed the substrates and/or products. Hence, a trapping agent that was compatible with the electrophilic oxonium ion was required. Cycloheptatriene, being a non-basic hydride donor, was selected for this purpose due to the very low hydride affinity (201 kcal/mol) of the tropylium cation.[40, 42] Treatment of a filtered CD_2Cl_2 solution of oxonium ions **24v**/**24v'**•$Al(pftb)_4$ at −20 °C with 1.1 eq. of cycloheptatriene followed by NMR monitoring showed that the oxonium ions **24v**/**24v'**•$Al(pftb)_4$ were virtually unreactive towards cycloheptatriene at −20 °C, but were rapidly reduced to **28**/**28'** at room temperature in 30 minutes. The reduction product **28**/**28'** was isolated as a 1.7:1 diastereomeric mixture in 42% yield (**Figure 5e**). Cycloheptatriene was therefore employed as a cation scavenger in the reaction between unfiltered **24v**/**24v'**•$Al(pftb)_4$ and silyl ketene acetal in CH_2Cl_2, in which the desired oxocane products **29** and **29'** were obtained in 81% total yield in 1.6:1 diastereomeric ratio. Reaction with other types of π-nucleophiles such as methallyltrimethylsilane, furan, 2-methylfuran and *N*-methyl pyrrole provided the corresponding adducts **30**-**33**, respectively (**Figure 5f**); see Supplementary Information page S70 onwards for more examples of oxonium ion quenching with various nucleophiles.

The oxonium ions **24q**•$Al(pftb)_4$ and **24r**•$Al(pftb)_4$ that were generated as single diastereomers most likely also underwent stereochemical equilibration *via* path *c* as with oxonium **24v**•$Al(pftb)_4$. Although the incipient tertiary benzyl cations in **24q**•$Al(pftb)_4$ and **24r**•$Al(pftb)_4$ were expected to have a higher hydride affinity compared to the *p*-methoxybenzyl cation in **24v**•$Al(pftb)_4$, the equilibration most likely was driven by the tendency to put the sterically more demanding enoate and enal groups pseudoequatorial.[43] This may also explain the tendency for disubstituted propargyl oxonium ions **24s-u**•$Al(pftb)_4$ to be generated as a mixture of diastereomers due to the small size of the propargyl group.

For the monosubstituted propargyl and enoate oxonium ions **24c**•$Al(pftb)_4$ and **24d**•$Al(pftb)_4$, although they were both found to resolve to a single diastereomer by prolonged incubation at 40 °C, or simply by leaving the sample at room temperature for several days for **24c**•$Al(pftb)_4$, decomposition of the oxonium ions was evident. This was suggested by the darkening of the sample, and a gradual reduction of their ^1H NMR signal intensity along with the appearance of broad resonances. The higher temperature required for these oxonium ions to undergo equilibration could be attributed to the requirement for the formation of incipient carbenium ions that have relatively high gas phase hydride affinities.

Properties of the oxonium ions: Rearrangement reactions

Although it was possible to acquire most of the NMR spectroscopic data of the monosubstituted oxonium ions **24a**•SbF_6 and **24b-24j**•$Al(pftb)_4$ at 298 K in CD_2Cl_2, some of the oxonium ions were unstable at this temperature. Notably, oxonium ion **24f**•$Al(pftb)_4$ was found to undergo rearrangement into oxocarbenium ion **35**•$Al(pftb)_4$ at temperatures above −20 °C (**Figure 6**).[44, 45] The oxocarbenium ion **35**•$Al(pftb)_4$ was characterised by NMR spectroscopy, with the ^{13}C NMR chemical

shift of the orange oxocarbenium ion carbon resonating at 245.4 ppm within the 240-250 ppm range known for oxocarbenium ions.[15, 46, 47] In addition, ^{1}H-^{13}C HMBC correlations between said carbon and the blue, brown, magenta, cyan and grey protons were observed. The formation of oxocarbenium ion **35**•Al(pftb)$_4$ from oxonium ion **24f**•Al(pftb)$_4$ suggests that oxonium ion-carbenium ion equilibrium by path *b* is accessible for this oxonium ion with the carbenium ion **26f**•Al(pftb)$_4$ undergoing reduction by an intramolecular hydride transfer pathway through the transition state **34**•Al(pftb)$_4$ to provide the oxocarbenium ion **35**•Al(pftb)$_4$.[48-53] The corresponding deuterated oxonium ion **24f**-*d*•Al(pftb)$_4$ gave the oxocarbenium ion **35**-*d*•Al(pftb)$_4$ with deuterium at the benzylic position in keeping with the mechanism proposed above (**Figure 6b**). The resulting oxocarbenium ions **35**•Al(pftb)$_4$ and **35**-*d*•Al(pftb)$_4$ were derivatised into ketones **36**/**36**-*d* with tetrabutylammonium bromide and tetrahydrofurans **37**/**37**-*d* with cycloheptatriene. To further elucidate the mechanism of this rearrangement reaction, the hydride transfer of oxonium ion **24f**•Al(pftb)$_4$ and the deuteride transfer of its deuterated analogue **24f**-*d*•Al(pftb)$_4$ were monitored by NMR spectroscopy at 10 °C in CD_2Cl_2. Both hydride and deuteride transfer reactions were found to be first-order with respect to the oxonium ions **24f**•Al(pftb)$_4$ and **24f**-*d*•Al(pftb)$_4$ respectively as expected with a modest kinetic isotope effect k_H/k_D = 1.48 ± 0.08 being measured from separate experiments suggesting that the C−H cleavage event is rate determining (see Supplementary Information page S88).[54] DFT calculations support this interpretation. The calculated transition state for the hydride transfer is chair-shaped with a C–H–C bond angle of 140° along the transferring axis (see Supplementary Information pages S110-S111). Consistent with an exothermic/exergonic step in forming the oxocarbenium ion **35**, H-transfer is highly asynchronous with a breaking C–H distance of 1.17 Å and a forming distance of 1.71 Å. These two factors result in a relatively small primary kinetic isotope effect calculated to be k_H/k_D = 1.85 in qualitative agreement with experiment (see reference 40 pages 425-428).

The propargylallyl oxonium ions **24o**•Al(pftb)$_4$ underwent rearrangement to provide the conjugated oxocarbenium ion **40**•Al(pftb)$_4$ *via* the proposed mechanism shown below which we have termed a Friedel-Crafts pinacol reaction, akin to the Prins-pinacol reaction (**Figure 7a**).[55, 56] It was possible to briefly observe the propargylallyl oxonium ion **24o**•Al(pftb)$_4$ by NMR spectroscopy at room temperature immediately after its generation, and its conversion to the oxocarbenium ion **40**•Al(pftb)$_4$ was monitored over time. Performing the halide abstraction at −10 °C followed by NMR data acquisition at the same temperature allowed observation of the propargylallyl oxonium ion **24o**•Al(pftb)$_4$ along with the proposed intermediate oxocarbenium ion **39**•Al(pftb)$_4$ in 2.4:1 ratio, providing another piece of evidence for the proposed mechanism leading to the formation of **40**•Al(pftb)$_4$ (see Supplementary Information pages S54-S55 for the spectroscopic assignments of **39**•Al(pftb)$_4$ and **40**•Al(pftb)$_4$). On the other hand, the propargylbenzyl oxonium ion **24w**•Al(pftb)$_4$ was not observed at room temperature and the oxocarbenium ion **42**•Al(pftb)$_4$ was the only species observed immediately after halide abstraction of the precursor **23w** (**Figure 7b).** It was subsequently found that resonances in keeping with the formation oxonium ion **24w**•Al(pftb)$_4$ could be observed by ^{1}H NMR at -40 °C but readily decayed with concomitant increase in the intensity of the resonances

of oxocarbenium ion **42w•**Al(pftb)$_4$ (see Supplementary Information page S55 for the spectroscopic assignment of **42•**Al(pftb)$_4$ and pages S67-S68 for the conversion of **24w•**Al(pftb)$_4$ into **42w•**Al(pftb)$_4$)). Reaction of the oxocarbenium ion **42•**Al(pftb)$_4$ with tetrabutylammonium bromide (open to air) surprisingly gave fulvenes **43** as the only identifiable product in 28% yield, presumably *via* an isomerisation-oxidation pathway (**Figure 7c**). The Friedel-Crafts pinacol reaction is not limited to the propargylallyl and propargylbenzyl oxonium ions **24o•**Al(pftb)$_4$ and **24w•**Al(pftb)$_4$. The allylbenzyl oxonium ion **24n•**Al(pftb)$_4$ was also found to undergo such rearrangement upon warming from −40 °C to room temperature (**Figure 7d**).This provided the oxocarbenium ions **46•**Al(pftb)$_4$ as a mixture of diastereomers and subsequent reaction of this species with tetrabutylammonium bromide gave the cyclopentanes **47** in 64% yield (see Supplementary Information page S55-S56 for the spectroscopic assignment of **46•**Al(pftb)$_4$). DFT calculations supported the proposed Friedel-Crafts pinacol rearrangement mechanism from oxonium ions **24o**, **24w** and **24n** *via* the corresponding carbenium ions **26o**, **26w** and **26n (**see Supplementary Information pages S111-S113). Interestingly, the formation of the oxocarbenium ions **39**, **42** and **46** from the corresponding carbenium ions is calculated to occur in a single elementary step. However, this process is highly asynchronous: C–C formation begins to occur in each TS, while 1,2-migration does not begin to occur until later along the Intrinsic Reaction Coordinate (IRC). This concerted, asynchronous mechanism avoids the intermediacy of a high-energy linear or secondary carbocation.

Substitution of the propargyl and allyl groups in the oxonium ions **24o** and **24n** with a phenyl group gave rise to benzylallyl and bisbenzyl oxonium ions **24m** and **24l**. Although these two oxonium ions could be spectroscopically captured and characterised at lower temperatures (with SbF_6^- as counteranion: –20 °C for **24m** and –30 °C for **24l**; with Al(pftb)$_4^-$ as counteranion: 0 °C for **24m** and –20 °C for **24l**), they were found to undergo efficient intramolecular Friedel-Crafts alkylation at room temperature with SbF_6^- as their counteranion. This is followed by opening of the tetrahydrofuran rings to provide the compounds **52** and **53**, which could be neutralised by Et_3N to provide the substituted dihydronaphthalenes **54** and **55** in 61% and 68% yields, respectively. (**Extended Data Figure 1**).

However, generation of the benzylallyl oxonium ion **24m•**Al(pftb)$_4$ with AgAl(pftb)$_4$·CH_2Cl_2 at room temperature did not result in efficient Friedel-Crafts reactivity. The oxonium ion **24m•**Al(pftb)$_4$ was found to be persistent for ~30 minutes before signatures of Friedel-Crafts reaction began to appear in its ^{1}H NMR spectrum with further decomposition of the oxonium ion **24m•**Al(pftb)$_4$ into uncharacterisable species also observed. The difference in behaviour of the oxonium ion **24m** with different counteranions may relate to how readily the Wheland intermediate undergoes rearomatisation after attack of the aryl ring onto the allylic cation in **26m** and benzylic cation in **26l** (the pK_a of an arenium ion is estimated to be −24.3)[57] which drives the reaction forward, therefore outcompeting potential decomposition pathways.

The oxonium ion **24l•**Al(pftb)$_4$ that was generated with AgAl(pftb)$_4$·CH_2Cl_2 at 0 °C and then warmed to room temperature gave rise to a 1,4-aryl transfer reaction (**Extended Data Figure 2**). The

oxocarbenium ion **59**•Al(pftb)$_4$ generated from the 1,4-aryl transfer reaction was characterized by NMR spectroscopy and was found to bear similar spectroscopic features with respect to oxocarbenium ion **35**•Al(pftb)$_4$ (see Supplementary Information page S53). The oxocarbenium ion **59**•Al(pftb)$_4$ could be trapped by tetrabutylammonium bromide after filtration to give the ketone **60** in 21% yield, along with a Friedel-Crafts product **61** which was isolated in 42% yield as a mixture of diastereomers (*d.r.* ~ 4:1). The generation of the Friedel-Crafts product **61** as a major product was not obvious from inspection of the ^{1}H and ^{13}C NMR spectrum of oxocarbenium ion **59**•Al(pftb)$_4$; however, broad resonances were present in the ^{1}H NMR spectrum of oxocarbenium ion **59**•Al(pftb)$_4$, which may indicate that **59**•Al(pftb)$_4$ is in equilibrium with other species such as the carbenium ions **57**•Al(pftb)$_4$ or **58**•Al(pftb)$_4$. The quenching of the carbenium ions **57**•Al(pftb)$_4$ and **58**•Al(pftb)$_4$ leads to aromatisation and therefore generates the observed Friedel-Crafts product **61**. The competing *ipso* and *ortho*-Friedel Crafts processes were investigated computationally. With the oxonium ion **24l** the transition states for *ipso*- and *ortho*- substitution (**26l** to **56** and **26l** to **57**) differ by ca. 1 kcal/mol with the pathway for *ipso*-substitution being lower in energy and directly giving the oxocarbenium ion **59** with the depicted phenonium ion **56** (**56**•Al(pftb)$_4$ in **Extended Data Figure 2**) being a transition state not an intermediate. By contrast with the oxonium ion **24m** *ortho*-substitution is favoured over *ipso*-substitution by 2 kcal/mol. Although the reaction pathways were readily mapped out using DFT calculations, the differing counterion dependent reaction outcomes are not readily explained (see Supplementary Information pages S113-S114).

Lastly, during the investigation of the synthesis of the parent allenylic oxonium ion **24x**•Al(pftb)$_4$, it was found that the observed product was the vinyl oxonium ion **62**•Al(pftb)$_4$ (**Figure 8**). Presumably, vinyl oxonium ion **62**•Al(pftb)$_4$ was generated from the attack of the ether oxygen at the allene central carbon, either directly or through oxonium-carbenium ion equilibrium with carbenium ion **26x**•Al(pftb)$_4$. The generation of the vinyl oxonium ion **62**•Al(pftb)$_4$ was most likely driven by the formation of a conjugated buta-1,3-diene unit. To the best of our knowledge, this constitutes the first example of a vinyl oxonium ion to be characterized by NMR spectroscopy (see Supplementary Information pages S116 for comparison between computed and calculated ^{1}H and ^{13} C NMR chemical shifts).

Conclusion

This paper outlines the synthesis and characterisation of twenty-two allylic, benzylic, propargylic and allenylic oxonium ions. Their synthesis enabled investigation of the fundamental properties of these oxonium ions, namely their stereochemical/conformational behaviour, tendency to undergo rearrangement reactions, and reactivity towards nucleophiles. These discoveries set the stage for further development of oxonium ion-based transformations.

Methods

The oxonium ions **24** were generated from their halide precursors **23** (1.0 eq.) and AgAl(pftb)$_4$·CH_2Cl_2 (or $AgSbF_6$) (1.1 eq.) in dry CD_2Cl_2 (0.7 mL) in a flame dried Young's NMR

tube at their respective *generation temperatures* (see **Figures 2** and **3**, and Supplementary Information, pages S38 to S51). The halide precursor **23** (1.0 eq.) was quickly weighed out directly into the flame-dried Young's NMR tube, followed by the addition of dry CD_2Cl_2 (0.3 mL). The cap of the Young's NMR tube was closed, and the solution was mixed thoroughly by vigorous shaking, and the solution was incubated at the respective *generation temperatures*. The silver salt ($AgAl(pftb)_4 \cdot CH_2Cl_2$ or $AgSbF_6$) (1.1 eq.) was weighed out separately in a flame dried round bottom flask in a nitrogen-filled glove bag and dissolved in dry CD_2Cl_2 (0.4 mL) at room temperature. The room temperature solution of the silver salt was rapidly injected into the solution of the halide precursor **23** through the opening of the Young's NMR tube (not the opening of the cap). The cap of the Young's NMR tube was then closed, and the reaction mixture was thoroughly mixed by vigorous shaking. The silver halide precipitate generated upon the formation of monosubstituted oxonium ions **24** was allowed to settle at the bottom of the Young's NMR tube at their *generation temperatures*. The monosubstituted oxonium ions **24** were then observed by NMR spectroscopy at their respective *acquisition temperatures*.

Data availability

The data (experimental procedures, characterisation data, NMR spectra, and computational methods and results for oxonium ion characterisation) supporting the findings of this study are available within the article and its supplementary information.

Acknowledgements

J.L.S. is grateful to the Royal Commission for the Exhibition of 1851 for an Industrial Fellowship and the generous support provided by that fellowship, as well as to the EPSRC Centre for Doctoral Training in Synthesis for Biology and Medicine (EP/L015838/1) for a studentship, generously supported by AstraZeneca, Diamond Light Source, Defence Science and Technology Laboratory, Evotec, GlaxoSmithKline, Janssen, Novartis, Pfizer, Syngenta, Takeda, UCB and Vertex. D.S.B. is grateful to the BBSRC and Syngenta for the award of an iCASE (BB/P504890/1). R.S.P. acknowledges support from the National Science Foundation (NSF CHE1955876) and the Alpine HPC resource, which is jointly funded by the University of Colorado Boulder, the University of Colorado Anschutz, and Colorado State University, and the Advanced Cyberinfrastructure Coordination Ecosystem: Services & Support (ACCESS) through allocation TG-CHE180056. We thank Prof. M. Mascal (UC Davis) and Dr N. Hafezi (UC Davis) for productive discussions regarding NMR assignment of oxonium ions.

Author Contributions

J.W.B and H.S.S.C designed the project. H.S.S.C., J.L.S and D.B. conducted the synthetic experiments. Y.L. and R.S.P. designed and performed the computational study. H.S.S.C., J.W.B. and R.S.P. wrote the paper with contributions from all the authors. All authors interpreted the results in the paper.

Competing Interests

The authors declare no competing interests.

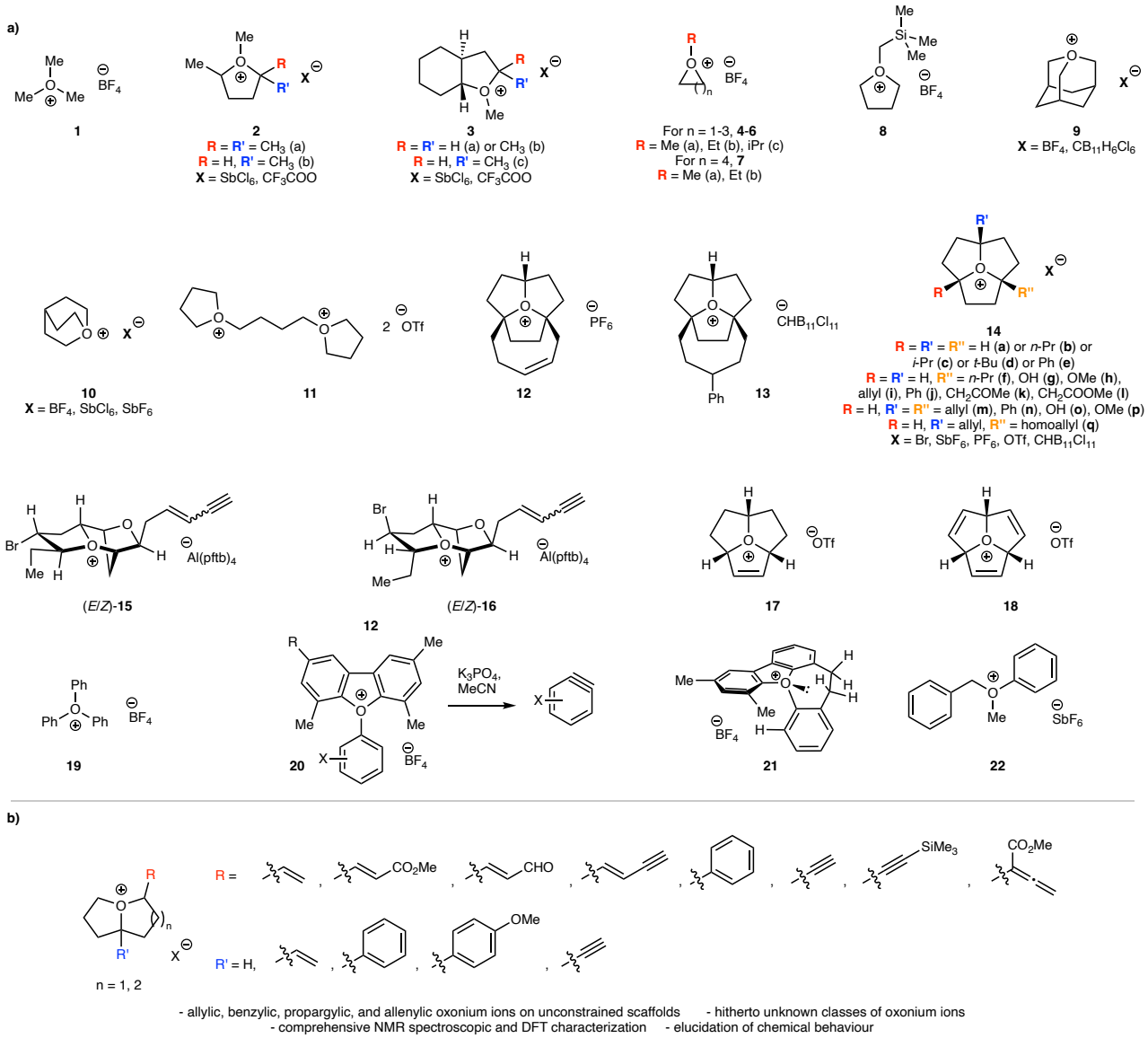

Figure 1. Literature examples of trialkyl and (tri)aryloxonium ions and oxonium ions from this study. a) A brief overview of reported trialkyloxonium ions[1-15] and some (tri)aryloxonium ions[16-18,22,33]. Please consult respective publications for the case-specific ion-pairings of oxonium ions **14a**–**14q**. **b)** Examples of oxonium ions described in this work. Tf = triflate = SO_2CF_3; pftb = perfluoro-*tert*-butoxy = $(CF_3)_3CO$.

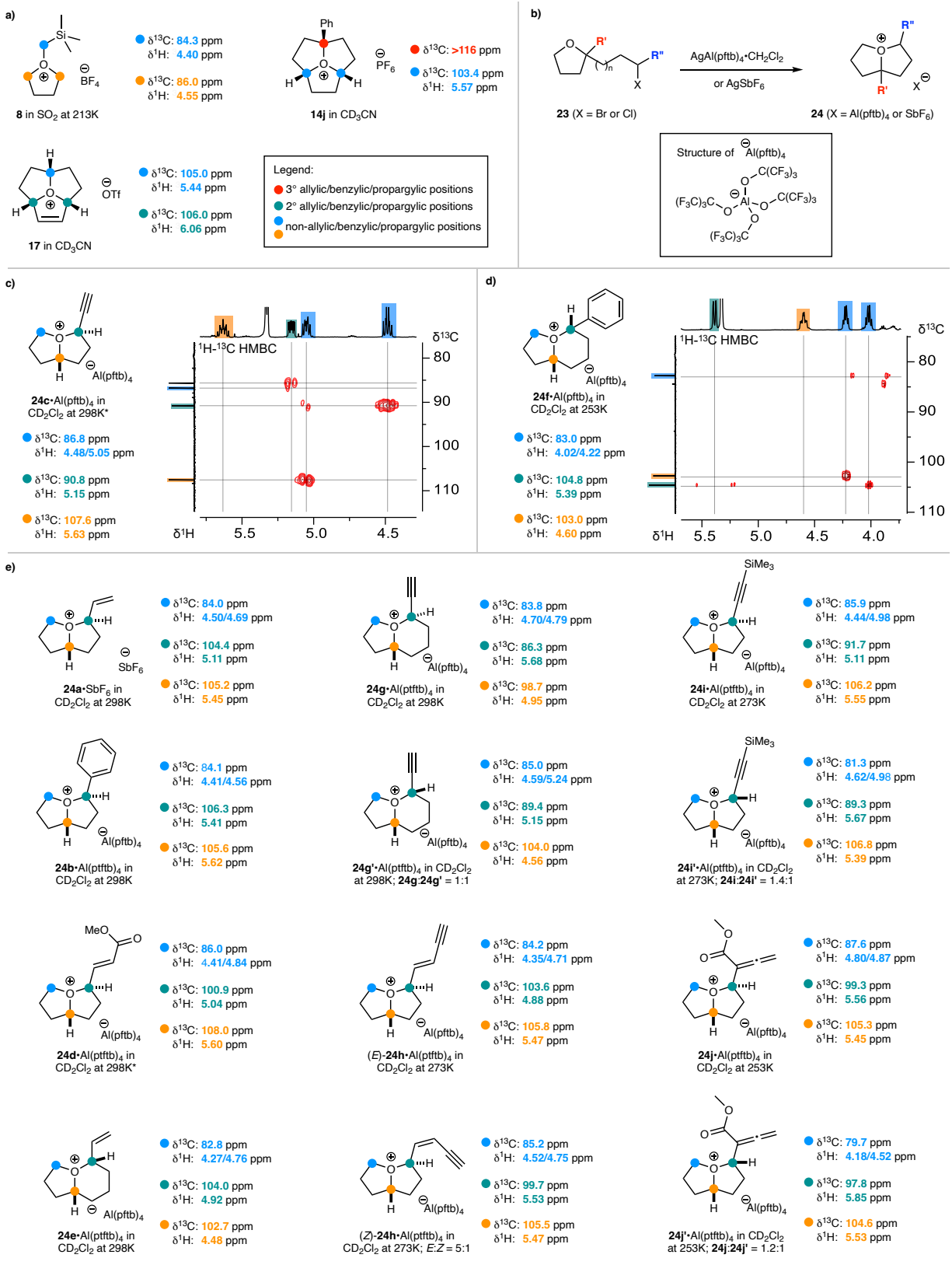

Figure 2. Synthesis and NMR characterisation/comparison of oxonium ions bearing an unsaturated substituent. a) ^{1}H and ^{13}C NMR data of literature oxonium ions: **8**, benzylic oxonium ion **14j** and allylic oxonium ion **17**. **b)** Generation of oxonium ions **24** from **23** *via* halide abstraction for NMR analysis. Reagents and conditions: 1.1 eq. $AgAl(pftb)_4 \cdot CH_2Cl_2$ or 1.1 eq. $AgSbF_6$, CD_2Cl_2, refer to **c**–**e)** for reaction and characterization temperature, which are identical unless otherwise specified. **c)** and **d)** Representative examples showcasing the characterization of monosubstituted oxonium ions

24c•Al(pftb)$_4$ and **24f•**Al(pftb)$_4$ by ^{1}H, ^{13}C and ^{1}H-^{13}C HMBC (Heteronuclear Multiple Bond Correlation) NMR spectroscopy. **e)** Examples of monosubstituted oxonium ions with their ^{1}H and ^{13}C NMR spectroscopic data. Their corresponding ^{1}H-^{13}C HMBC correlation data, presented in the form as in **c**–**d)** can be found in the SI. *Initially generated as a mixture of diastereomers, single diastereomer of **24c•**Al(pftb)$_4$ obtained slowly at room temperature or more rapidly by incubation at 40 °C (338K). For **24d•**Al(pftb)$_4$, single diastereomer obtained only after incubation at 40 °C (338K).

a)

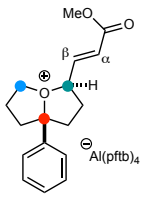

24r•Al(pftb)$_4$ in CD_2Cl_2 at 253K

- δ^{13}C: **85.7** ppm, δ^{1}H: **4.59/4.92** ppm
- δ^{13}C: **101.6** ppm, δ^{1}H: **5.14** ppm
- δ^{13}C: **123.5** ppm

C=O δ^{13}C: **164.8** ppm
α C-H δ^{13}C: **131.2** ppm, δ^{1}H: **6.37** ppm
β C-H δ^{13}C: **134.9** ppm, δ^{1}H: **6.94** ppm

ipso δ^{13}C: **137.2** ppm
ortho δ^{13}C: **123.8** ppm, δ^{1}H: **7.23** ppm
meta δ^{13}C: **130.0** ppm, δ^{1}H: **7.52** ppm
para δ^{13}C: **130.5** ppm, δ^{1}H: **7.52** ppm

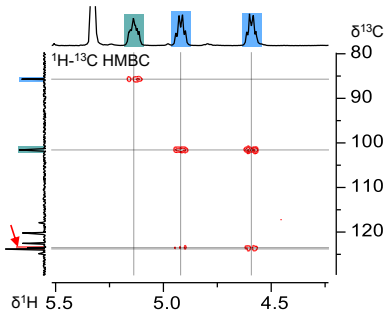

b)

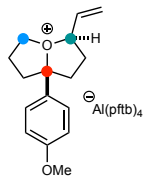

24p•Al(pftb)$_4$ in CD_2Cl_2 at 253K

- δ^{13}C: **83.4** ppm, δ^{1}H: **4.53/4.77** ppm
- δ^{13}C: **105.9** ppm, δ^{1}H: **4.97** ppm
- δ^{13}C: **121.2** ppm

Terminal CH_2 δ^{13}C: **129.6** ppm, δ^{1}H: **5.82** ppm
Internal C-H δ^{13}C: **128.7** ppm, δ^{1}H: **6.00** ppm

ipso δ^{13}C: **129.3** ppm
ortho δ^{13}C: **125.6** ppm, δ^{1}H: **7.15** ppm
meta δ^{13}C: **114.9** ppm, δ^{1}H: **6.98** ppm
para (OMe) δ^{13}C: **160.9** ppm

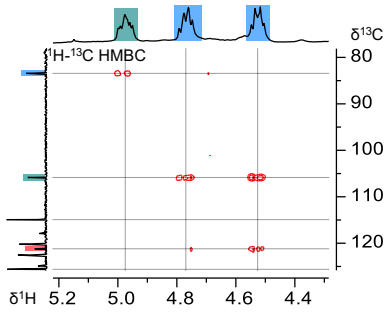

c)

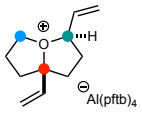

24k•Al(pftb)$_4$ in CD_2Cl_2 at 273K

- δ^{13}C: **83.2** ppm, δ^{1}H: **4.38/4.68** ppm
- δ^{13}C: **105.4** ppm, δ^{1}H: **4.88** ppm
- δ^{13}C: **119.4** ppm

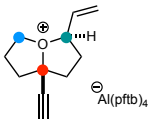

24o•Al(pftb)$_4$ in CD_2Cl_2 at 263K#

- δ^{13}C: **83.5** ppm, δ^{1}H: **4.34/4.82** ppm
- δ^{13}C: **106.0** ppm, δ^{1}H: **4.88** ppm
- δ^{13}C: **110.4** ppm

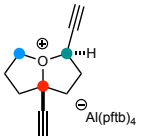

24t•Al(pftb)$_4$ in CD_2Cl_2 at 298K

- δ^{13}C: **86.5** ppm, δ^{1}H: **4.45/5.15** ppm
- δ^{13}C: **91.0** ppm, δ^{1}H: **5.15** ppm
- δ^{13}C: **114.8** ppm

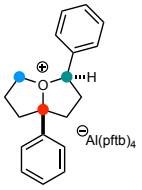

24l•Al(pftb)$_4$ in CD_2Cl_2 at 253K

- δ^{13}C: **84.0** ppm, δ^{1}H: **4.63/4.69** ppm
- δ^{13}C: **107.8** ppm, δ^{1}H: **5.57** ppm
- δ^{13}C: **119.8** ppm

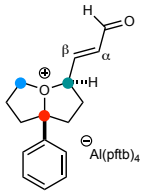

24q•Al(pftb)$_4$ in CD_2Cl_2 at 253K

- δ^{13}C: **86.5** ppm, δ^{1}H: **4.64/4.97** ppm
- δ^{13}C: **100.6** ppm, δ^{1}H: **5.25** ppm
- δ^{13}C: **125.4** ppm

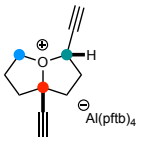

24t'•Al(pftb)$_4$ in CD_2Cl_2 at 298K, **24t**:**24t'** = 1 : 1.1

- δ^{13}C: **81.8** ppm, δ^{1}H: **4.84/5.02** ppm
- δ^{13}C: **88.1** ppm, δ^{1}H: **5.81** ppm
- δ^{13}C: **115.0** ppm

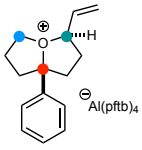

24m•Al(pftb)$_4$ in CD_2Cl_2 at 273K

- δ^{13}C: **84.0** ppm, δ^{1}H: **4.58/4.84** ppm
- δ^{13}C: **106.7** ppm, δ^{1}H: **5.06** ppm
- δ^{13}C: **119.4** ppm

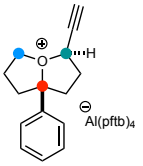

24s•Al(pftb)$_4$ in CD_2Cl_2 at 273K

- δ^{13}C: **87.1** ppm, δ^{1}H: **4.68/5.17** ppm
- δ^{13}C: **91.4** ppm, δ^{1}H: **5.32** ppm
- δ^{13}C: **123.4** ppm

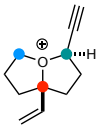

24u•Al(pftb)$_4$ in CD_2Cl_2 at 273K

- δ^{13}C: **86.2** ppm, δ^{1}H: **4.46/5.05** ppm
- δ^{13}C: **90.0** ppm, δ^{1}H: **5.15** ppm
- δ^{13}C: **123.6** ppm

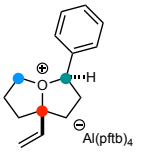

24n•Al(pftb)$_4$ in CD_2Cl_2 at 233K

- δ^{13}C: **83.1** ppm, δ^{1}H: **4.42/4.50** ppm
- δ^{13}C: **106.0** ppm, δ^{1}H: **5.38** ppm
- δ^{13}C: **119.2** ppm

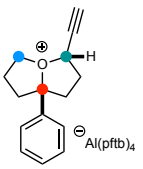

24s'•Al(pftb)$_4$ in CD_2Cl_2 at 273K, **24s**:**24s'** = 1.3 : 1

- δ^{13}C: **82.5** ppm, δ^{1}H: **4.89/5.32** ppm
- δ^{13}C: **88.5** ppm, δ^{1}H: **5.88** ppm
- δ^{13}C: **123.2** ppm

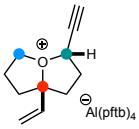

24u'•Al(pftb)$_4$ in CD_2Cl_2 at 273K, **24u**:**24u'** = 1.2 : 1

- δ^{13}C: **81.5** ppm, δ^{1}H: **4.72/5.03** ppm
- δ^{13}C: **87.3** ppm, δ^{1}H: **5.69** ppm
- δ^{13}C: **123.1** ppm

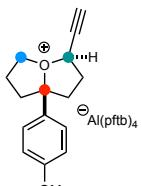

24v•Al(pftb)$_4$ in CD_2Cl_2 at 233K*

- δ^{13}C: **84.0** ppm, δ^{1}H: **4.44/4.94** ppm
- δ^{13}C: **87.1** ppm, δ^{1}H: **5.13** ppm
- δ^{13}C: **140.8** ppm

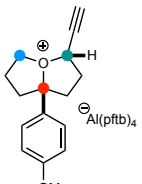

24v'•Al(pftb)$_4$ in CD_2Cl_2 at 233K*, **24v**:**24v'** ~ 1.7 - 1.8 : 1

- δ^{13}C: **80.8** ppm, δ^{1}H: **4.77/5.06** ppm
- δ^{13}C: **86.3** ppm, δ^{1}H: **5.73** ppm
- δ^{13}C: **130.6** ppm

Figure 3. NMR characterisation of oxonium ions bearing unsaturation at two positions. a–b) Representative examples showcasing the characterization of disubstituted oxonium ions **24r•**Al(pftb)$_4$ and **24p•**Al(pftb)$_4$ by ^{1}H, ^{13}C and ^{1}H-^{13}C HMBC (Heteronuclear Multiple Bond Correlation) NMR spectroscopy. **c)** Examples of disubstituted oxonium ions with their ^{1}H and ^{13}C NMR spectroscopic data. Their corresponding ^{1}H-^{13}C HMBC correlation data, presented in the form as in **a**–**b)** can be found in the SI. *****Generated at 253K. $^{\#}$Oxonium ion **24o•**Al(pftb)$_4$ was generated as a ca. 2.4:1 mixture with oxocarbenium ion **52•**Al(pftb)$_4$ (see below).

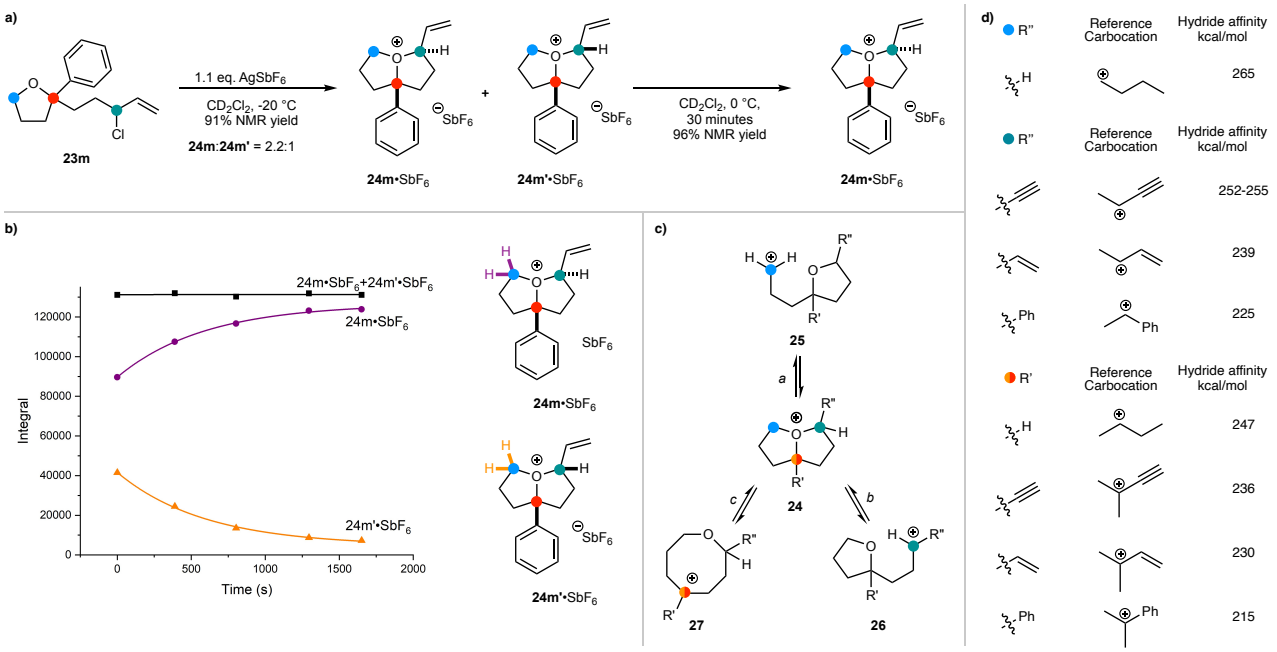

412

413 **Figure 4. Oxonium ion equilibration**. **a)** Generation of a mixture of **24m**•SbF_6 and **24m'**•SbF_6 from **23m** at −20 °C,
414 followed by equilibration to **24m**•SbF_6 at 0 °C (See full NMR characterization of **24m**•SbF_6 in the SI, full characterization
415 of **24m'**•SbF_6 was not attempted due to its low initial concentration and facile conversion into **24m**•SbF_6. The
416 identification of **24m'**•SbF_6 was by NMR spectroscopic comparison with oxonium ions **24m**•SbF_6 and **24s'**–
417 **24u'**•$Al(pftb)_4$). **b)** NMR monitoring of the conversion of **24m'**•SbF_6 to **24m**•SbF_6 at 0 °C. **c)** Three pathways for oxonium
418 ion-carbenium ion equilibrium. **d)** Gas phase hydride affinities of incipient carbenium ion **25**, **26** and **27**.

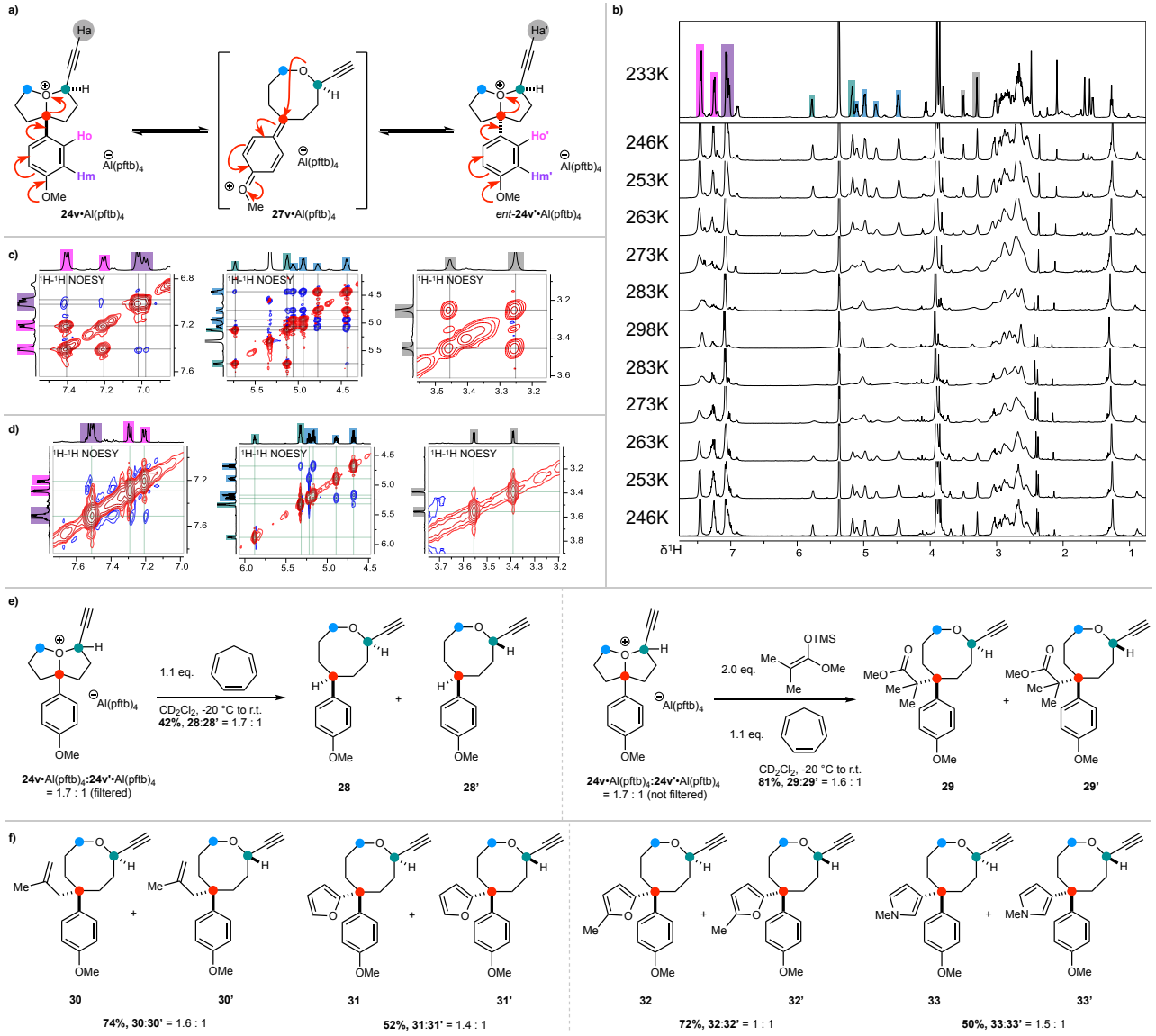

Figure 5. Characterisation and reactivity of oxonium ion 24v•Al(pftb)$_4$ showing fluxionality by NMR. **a)** Proposed mechanism for the observed exchange between **24v**•Al(pftb)$_4$ and *ent*-**24v'**•Al(pftb)$_4$. **b)** Reversible temperature dependence of chemical exchange between 246 K (−27 °C) and 298 K (25 °C). The ^{1}H NMR spectrum of **24v**•Al(pftb)$_4$ at 233 K (−40 °C) is displayed with the signals of interest highlighted. **c)** Excerpts of the ^{1}H-^{1}H NOESY spectrum of **24v**•Al(pftb)$_4$ at 233 K (−40 °C), showing exchange cross-peaks (red in colour, intense and same phase as the diagonal). **d)** Excerpts of the ^{1}H-^{1}H NOESY spectrum of **24s**•Al(pftb)$_4$ at 273 K (0 °C), showing the absence of exchange cross-peaks. **e)** Reaction of the oxonium ions **24v**•Al(pftb)$_4$ and **24v'**•Al(pftb)$_4$ with cycloheptatriene and silyl ketene acetal. Reagents and conditions: 1.1 eq. cycloheptatriene (or 2.0 eq. silyl ketene acetal and 1.1 eq. cycloheptatriene), CD_2Cl_2, −20 °C to r.t., reaction progress monitored by ^{1}H NMR spectroscopy or TLC analysis. **f)** Products of the reactions between oxonium ions **24v**•Al(pftb)$_4$ and **24v'**•Al(pftb)$_4$ with methallyltrimethylsilane, furan, 2-methylfuran, and *N*-methylpyrrole. Please refer to Supplementary Information for experimental conditions and stereochemical assignments. r.t. = room temperature; TLC = thin layer chromatography; TMS = trimethylsilyl = $(CH_3)_3Si$.

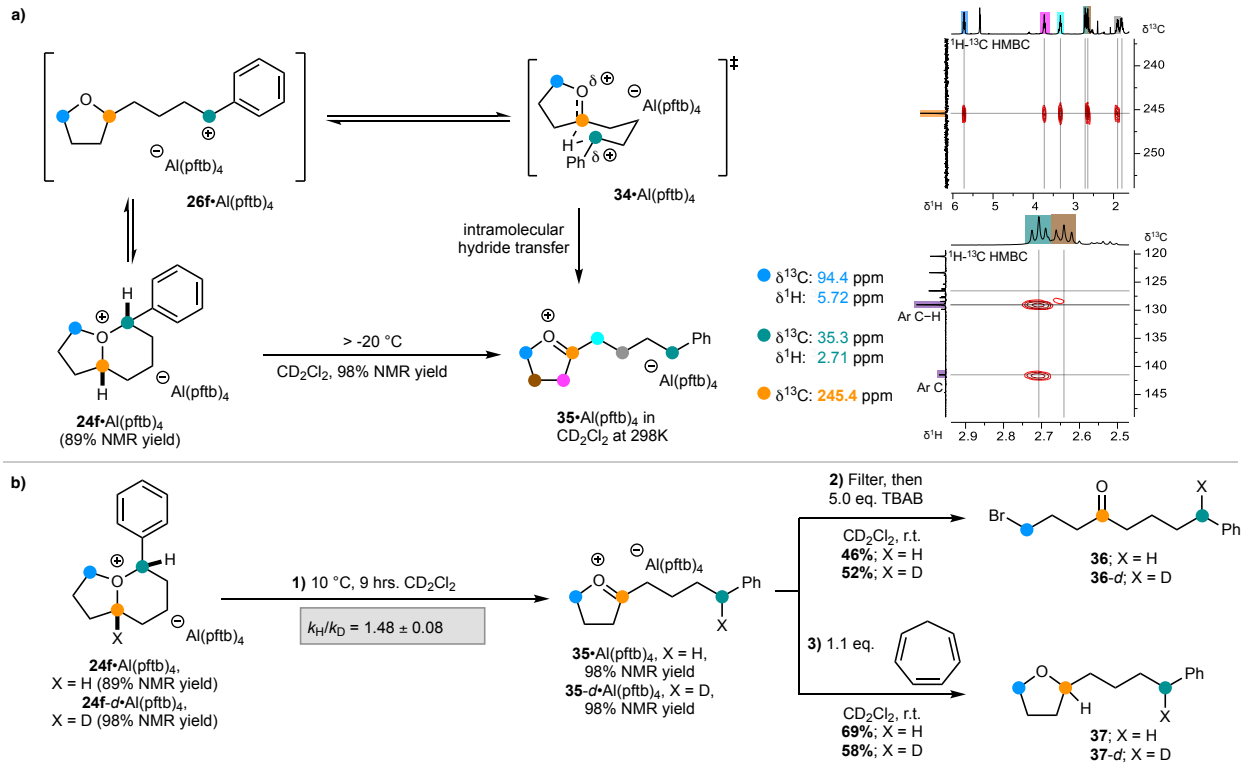

Figure 6. Rearrangement of a benzylic oxonium ion. a) Proposed mechanism for the formation of **35**•Al(pftb)$_4$ from **24f**•Al(pftb)$_4$. ^{1}H, ^{13}C NMR and ^{1}H-^{13}C HMBC (Heteronuclear Multiple-Bond Correlation) NMR data of **35**•Al(pftb)$_4$ are provided to support its structural assignment. **b)** Conversion of **24f**•Al(pftb)$_4$ and **24f**-*d*•Al(pftb)$_4$ to **35**•Al(pftb)$_4$ and **35**-*d*•Al(pftb)$_4$ and their derivatization into **36**/**37** and **36**-*d*/**37**-*d*. Reagents and conditions: **1)** 10 °C, CD_2Cl_2, 9 hrs, refer to figure for NMR yields. **2)** Filter off $AgCl_{(s)}$ precipitate at r.t., then add 5.0 eq. Tetrabutylammonium bromide (TBAB), CD_2Cl_2, r.t., refer to figure for isolated yields. **3)** 1.1 eq. cycloheptatriene, CD_2Cl_2, r.t., refer to figure for isolated yields.

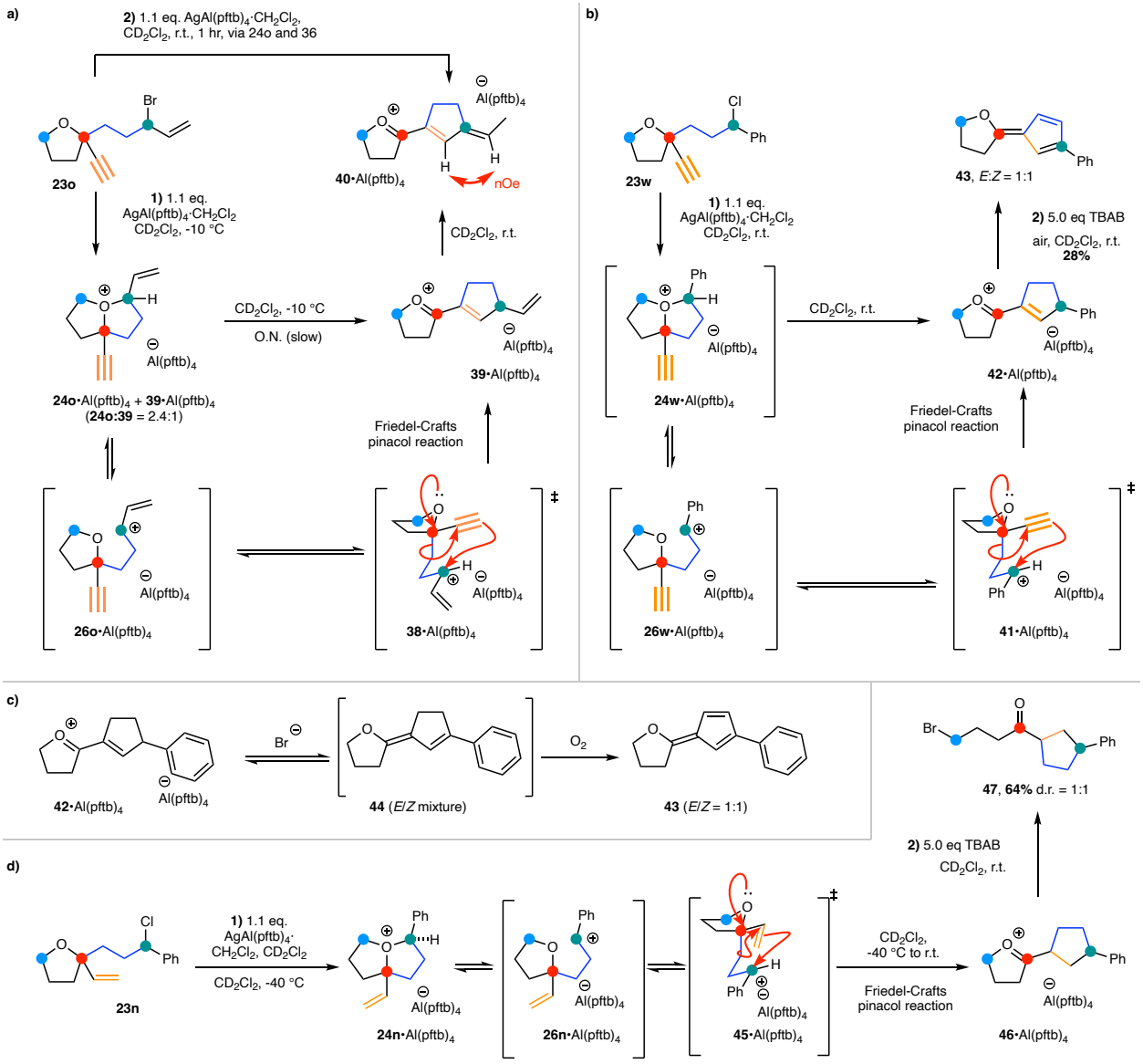

Figure 7. Rearrangement of propargylic oxonium ions. **a)** Formation of oxocarbenium ion **39**•Al(pftb)$_4$ from **23o** via the Friedel-Crafts pinacol reaction. Reagents and conditions: **1)** 1.1 eq. AgAl(pftb)$_4$·CH_2Cl_2, CD_2Cl_2, −10 °C, overnight (NMR acquisition), *then* r.t. **2)** 1.1 eq. AgAl(pftb)$_4$·CH_2Cl_2, CD_2Cl_2, r.t., 1 hr. **b)** Formation of oxocarbenium ion **42**•Al(pftb)$_4$ from **23w** via the Friedel-Crafts pinacol reaction. Reagents and conditions: **1)** 1.1 eq. AgAl(pftb)$_4$·CH_2Cl_2, CD_2Cl_2, r.t. **2)** 5.0 eq. tetrabutylammonium bromide (TBAB), air, CD_2Cl_2, r.t. 28%, *E*:*Z* = 1:1. **c)** A proposed mechanism for the formation of **43** from **42**•Al(pftb)$_4$. **d)** Formation of oxocarbenium ion **46**•Al(pftb)$_4$ from **23n** via the Friedel-Crafts pinacol reaction. Reagents and condition: **1)** 1.1 eq. AgAl(pftb)$_4$·CH_2Cl_2, CD_2Cl_2, −40 °C, overnight (NMR acquisition), *then* r.t. **2)** Filter off $AgCl_{(s)}$, 5.0 eq TBAB, CD_2Cl_2, r.t. 64% over 2 steps, *d.r.* = 1:1. O.N. = overnight; nOe = nuclear Overhauser effect; d.r. = diastereomeric ratio.

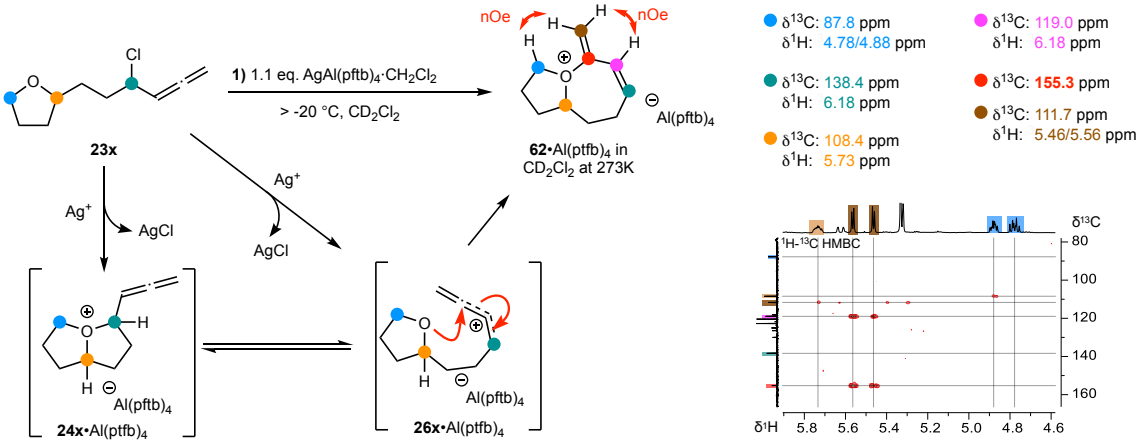

449

450 **Figure 8. Generation of vinyl oxonium ion 62•Al(pftb)$_4$ from 23x**. Reagents and conditions: 1.1 eq. AgAl(pftb)$_4$·CH_2Cl_2,
451 CD_2Cl_2, mixing of reagents at −20 °C, then warmed to above −20 °C for the generation of **62**•Al(pftb)$_4$. ^{1}H, ^{13}C NMR and
452 ^{1}H-^{13}C HMBC (Heteronuclear Multiple-Bond Correlation) NMR data of **62**•Al(pftb)$_4$ are provided to support its structural
453 assignment.

454

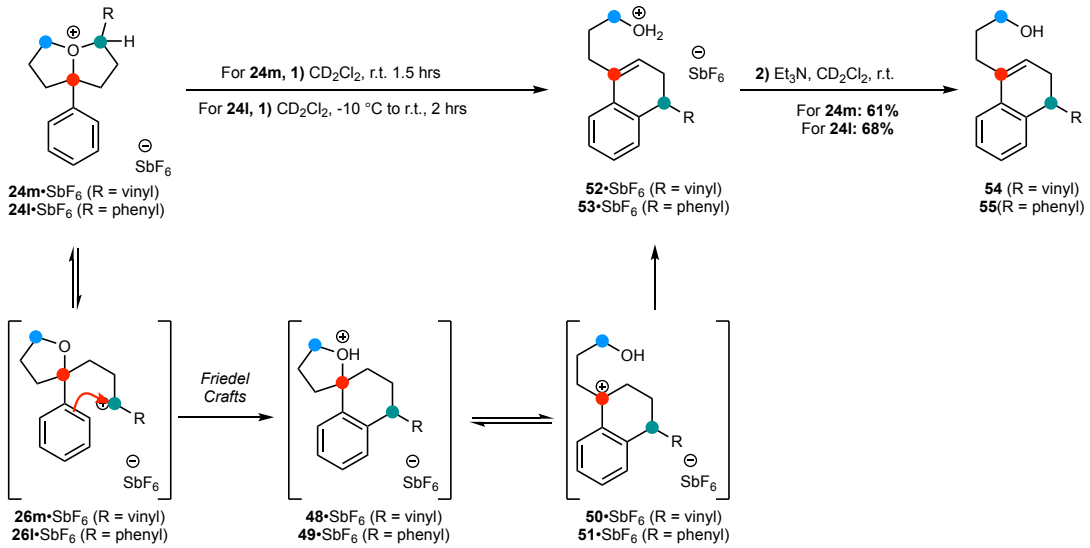

Extended Data Figure 1. Formation of Friedel-Crafts products 54 and 55 from oxonium ions 24m•SbF_6 and 24l•SbF_6. Reagents and conditions: For **24m**•SbF_6: **1)** CD_2Cl_2, r.t., 1.5 hrs. **2)** 2.0 eq. Et_3N, CD_2Cl_2, r.t., 61% over 2 steps. For **24l**•$Al(pftb)_4$: **1)** CD_2Cl_2, −10 °C to r.t., 2 hrs. **2)** 2.0 eq. Et_3N, CD_2Cl_2, r.t. 68% over 2 steps.

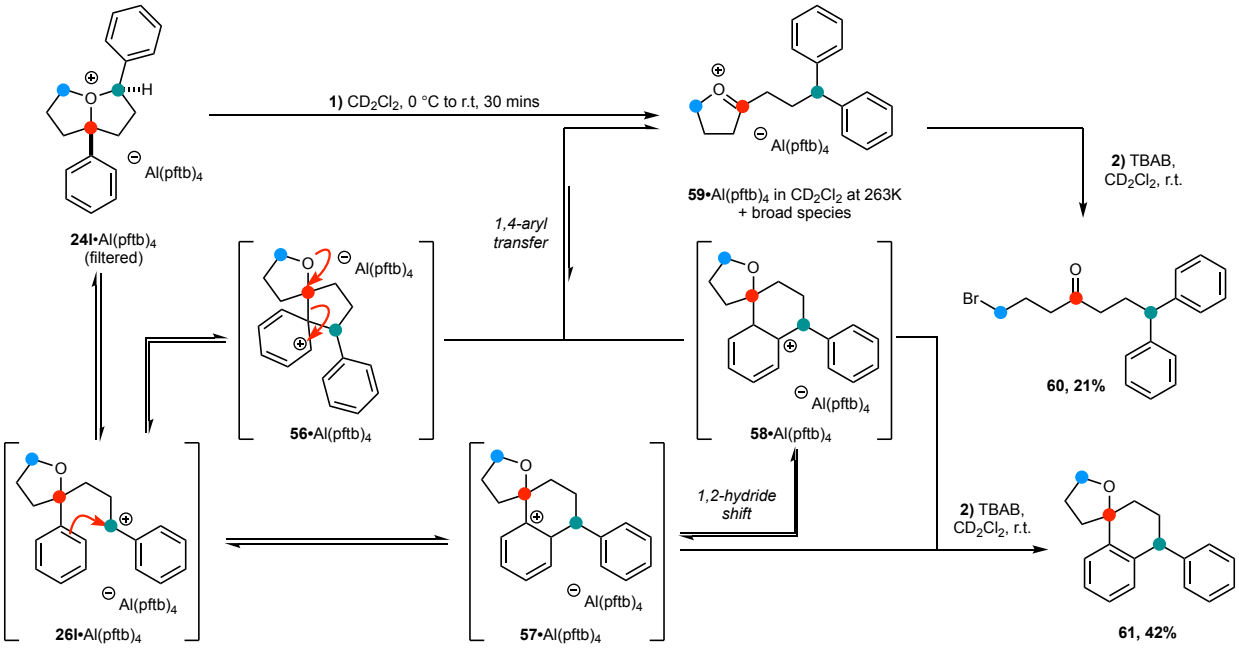

Extended Data Figure 2. Formation of 1,4-aryl transfer product 60 from oxonium ion 24l•Al(pftb)$_4$. Reagents and conditions: **1)** CD_2Cl_2, 0 °C to r.t., 30 minutes. **2)** Filter, then 5.0 eq. Tetrabutylammonium bromide, CD_2Cl_2, r.t. **60**: 21% over 2 steps, **61**: 42% over 2 steps (*d.r.* ~ 4:1).

References

(1) Meerwein, H.; Hinz, G.; Hofmann, P.; Kroning, E.; Pfeil, E. Über Tertiäre Oxoniumsalze, I. *J. Prakt. Chem.* **1937**, *147*, 257-285.

(2) Gargiulo, R. J.; Tarbell, D. S. Cyclic Oxonium Ions and Related Structures. *Proc. Natl. Acad. Sci. U. S. A.* **1969**, *62*, 52-55.

(3) Lambert, J. B.; Johnson, D. H. The stereochemistry and inversion of trivalent oxygen. *J. Am. Chem. Soc.* **1968**, *90*, 1349-1350.

(4) Klages, F.; Gordon, J. E.; Jung, H. A. NMR- und IR-Spektren von Oxoniumsalzen. *Chem. Ber.* **1965**, *98*, 3748-3756.

(5) Meerwein, H.; Battenberg, E.; Gold, H. Über Tertiäre Oxoniumsalze, II. *J. Prakt. Chem.* **1939**, *154*, 83-156.

(6) Etzkorn, M.; Aniszfeld, R.; Li, T.; Buchholz, H.; Rasul, G.; Prakash, G. K. S.; Olah, G. A. 1-Oxoniaadamantane. *Eur. J. Org. Chem.* **2008**, 4555-4558.

(7) Olah, G. A.; Doggweiler, H.; Felberg, J. D.; Frohlich, S. Onium ions. 33. (Trimethylsilyl)- and [(trimethylsilyl)methyl]oxonium and halonium ions. *J. Org. Chem.* **1985**, *50*, 4847-4851.

(8) Klages, F.; Jung, H. A.; Wagner, H. Synthese und Eigenschaften eines bicyclischen Oxoniumsalzes. *Chem. Ber.* **1965**, *98*, 3757-3764.

(9) Smith, S.; Schultz, W. J.; Newmark, R. A. New Aspects of the Chemistry of Living Tetrahydrofuran Polymers Initiated by Trifluoromethane Sulfonic Anhydride. In *Ring-Opening Polymerization*, ACS Symposium Series, Vol. 59; American Chemical Society, 1977; pp 13-23.

(10) Mascal, M.; Hafezi, N.; Meher, N. K.; Fettinger, J. C. Oxatriquinane and oxatriquinacene: extraordinary oxonium ions. *J. Am. Chem. Soc.* **2008**, *130*, 13532-13533.

(11) Stoyanov, E. S.; Gunbas, G.; Hafezi, N.; Mascal, M.; Stoyanova, I. V.; Tham, F. S.; Reed, C. A. The $R_3O^+ \bullet\bullet\bullet H^+$ hydrogen bond: toward a tetracoordinate oxadionium(2+) ion. *J. Am. Chem. Soc.* **2012**, *134*, 707-714.

(12) Gunbas, G.; Hafezi, N.; Sheppard, W. L.; Olmstead, M. M.; Stoyanova, I. V.; Tham, F. S.; Meyer, M. P.; Mascal, M. Extreme oxatriquinanes and a record C-O bond length. *Nat. Chem.* **2012**, *4*, 1018-1023.

(13) Gunbas, G.; Sheppard, W. L.; Fettinger, J. C.; Olmstead, M. M.; Mascal, M. Extreme oxatriquinanes: structural characterization of alpha-oxyoxonium species with extraordinarily long carbon-oxygen bonds. *J. Am. Chem. Soc.* **2013**, *135*, 8173-8176.

(14) Suzuki, H.; Muratake, H. Functionalized Oxatriquinanes and Their Structural Equilibrium in Protic Solvent. *Chem. Pharm. Bull.* **2014**, *62*, 921-926.

(15) Chan, H. S. S.; Nguyen, Q. N. N.; Paton, R. S.; Burton, J. W. Synthesis, Characterization, and Reactivity of Complex Tricyclic Oxonium Ions, Proposed Intermediates in Natural Product Biosynthesis. *J. Am. Chem. Soc.* **2019**, *141*, 15951-15962.

(16) Nesmeyanov, A. N.; Makarova, L. G.; Tolstaya, T. P. Heterolytic decomposition of onium compounds (diphenyl halogenonium and triphenyloxonium salts). *Tetrahedron* **1957**, *1*, 145-157.

(17) Nesmeyanov, A. N.; T. P. Tolstaya. Triphenyloxonium salts. *Dokl. Akad. Nauk SSSR* **1957**, *117*,

626-628.
(18) Smith, O.; Hindson, M. J.; Sreenithya, A.; Tataru, V.; Paton, R. S.; Burton, J. W.; Smith, M. D. Harnessing triaryloxonium ions for aryne generation. *Nat. Synth.* **2023**, *3*, 58-66.
(19) Chen, W. L.; Fang, S.; Song, J. L.; Hu, Q.; Zhang, S. S.; Shu, B. Base-Promoted Sulfur Arylation of Sulfenamides to Oxonium Aryne Precursors: Chemoselective Synthesis of Sulfilimines and o-Sulfanylanilines. *J. Org. Chem.* **2025**, *90*, 448-457.
(20) Hellwinkel, D.; Seifert, H. Zur Frage des pentakoordinierten Stickstoffs: Reaktionen von (spiro)cyclischen Tetraarylammonium-Salzen mit Nucleophilen. *Justus Liebigs Ann. Chem.* **1972**, *762*, 29-54.
(21) Tolstaya, T. P.; Tsariev, D. A.; Luzikov, Y. N. Reaction of triaryloxonium salts with bases via dehydroarenes. *Tetrahedron Lett.* **1997**, *38*, 4457-4458.
(22) Smith, O.; Popescu, M. V.; Hindson, M. J.; Paton, R. S.; Burton, J. W.; Smith, M. D. Control of stereogenic oxygen in a helically chiral oxonium ion. *Nature* **2023**, *615*, 430-435.
(23) Fleming, I. Molecular Orbitals and Organic Chemical Reactions. John Wiley & Sons, Ltd: Chichester, UK, 2010; p 181.
(24) Wu, C.-H.; Galabov, B.; Wu, J. I. C.; Ilieva, S.; von R. Schleyer, P.; Allen, W. D. Do π-Conjugative Effects Facilitate SN2 Reactions? *J. Am. Chem. Soc.* **2014**, *136*, 3118-3126.
(25) Robiette, R.; Trieu-Van, T.; Aggarwal, V. K.; Harvey, J. N. Activation of the SN2 Reaction by Adjacent pi Systems: The Critical Role of Electrostatic Interactions and of Dissociative Character. *J. Am. Chem. Soc.* **2016**, *138*, 734-737.
(26) Zhang, J.; Liao, Z.; Chen, L.; Zhu, S. Rapid Access to Oxa-Bridged Bicyclic Skeletons through Gold-Catalyzed Tandem Rearrangement Reaction. *Chem. Eur. J.* **2019**, *25*, 9405-9409.
(27) Dean, A. C.; Randle, E. H.; Lacey, A. J. D.; Marczak Giorio, G. A.; Doobary, S.; Cons, B. D.; Lennox, A. J. J. Alkene 1,3-Difluorination via Transient Oxonium Intermediates. *Angew. Chem. Int. Ed. Engl.* **2024**, *63*, e202404666.
(28) Uemura, M.; Watson, I. D. G.; Katsukawa, M.; Toste, F. D. Gold(I)-Catalyzed Enantioselective Synthesis of Benzopyrans via Rearrangement of Allylic Oxonium Intermediates. *J. Am. Chem. Soc.* **2009**, *131*, 3464-3465.
(29) Das, G. K.; Mandal, S. C.; Mondal, N. Study on First Reported (2,5) ene Cyclisation: Does it Really Follow a Concerted Pathway? *J. Chem. Res.* **2003**, 588-590.
(30) Liu, H.; Laporte, A. G.; Gonzalez Pinardo, D.; Fernandez, I.; Hazelard, D.; Compain, P. An Unexpected Lewis Acid-Catalyzed Cascade during the Synthesis of the DEF-Benzoxocin Ring System of Nogalamycin and Menogaril: Mechanistic Elucidation by Intermediate Trapping Experiments and Density Functional Theory Studies. *J. Org. Chem.* **2024**, *89*, 5634-5649.
(31) Okamoto, K.; Kinoshita, T.; Shingu, H. The Retentive Solvolysis. VII. Structural Effect of Leaving Group on the Steric Course of the S_N1 Phenolysis of 1-Phenylethyl Systems. *Bull. Chem. Soc. Jpn.* **1970**, *43*, 1545-1553.
(32) Słomkowski, S.; Penczek, S. The carbenium ⇄ oxonium ion equilibrium. Part I. Reversible reaction of non-paired triphenylmethyl cation with ethers and acetals. *J. Chem. Soc., Perkin Trans. 2*

1974, 1718-1722.
(33) Olah, G. A.; Olah, J. A.; Ohyama, T. Friedel-Crafts alkylation of anisole and its comparison with toluene. Predominant ortho-para substitution under kinetic conditions and the effect of thermodynamic isomerizations. *J. Am. Chem. Soc.* **1984**, *106*, 5284-5290.
(34) Chan, H. S. S.; Thompson, A. L.; Christensen, K. E.; Burton, J. W. Forwards and backwards – synthesis of Laurencia natural products using a biomimetic and retrobiomimetic strategy incorporating structural reassignment of laurefurenynes C–F. *Chem. Sci.* **2020**, *11*, 11592-11600.
(35) Krossing, I. The facile preparation of weakly coordinating anions: structure and characterisation of silverpolyfluoroalkoxyaluminates $AgAl(OR_F)_4$, calculation of the alkoxide ion affinity. *Chem. Eur. J.* **2001**, *7*, 490-502.
(36) Allinger, N. L.; Coke, J. L. The Relative Stabilities of cis and trans Isomers. VII. The Hydrindanes. *J. Am. Chem. Soc.* **1960**, *82*, 2553-2556.
(37) Farrant, R. D.; Hollerton, J. C.; Lynn, S. M.; Provera, S.; Sidebottom, P. J.; Upton, R. J. NMR quantification using an artificial signal. *Magn. Reson. Chem.* **2010**, *48*, 753-762.
(38) Rappoport, Z.; Stang, P. J. Dicoordinated carbocations. Wiley: Chichester; New York, 1997; pp 126-129.
(39) Aue, D. H.; Bowers, M. T. Chapter 9 - Stabilities of positive ions from equilibrium gas-phase basicity measurements. In *Gas Phase Ion Chemistry*, Bowers, M. T. Ed.; Academic Press, 1979; pp 31-59.
(40) Anslyn, E. V.; Dougherty, D. A. *Modern Physical Organic Chemistry*; University Science Books: Sausalito, 2006; p^pp 87-88.
(41) Hansch, C.; Leo, A.; Taft, R. W. A survey of Hammett substituent constants and resonance and field parameters. *Chem. Rev.* **1991**, *91*, 165-195.
(42) Kimura, T.; Takahashi, T.; Nishiura, M.; Yamamura, K. Novel Metal-Free Hydrogenation of the Carbon−Carbon Double Bond in Azulenoid Enones by Use of Cycloheptatriene and Protic Acid. *Org. Lett.* **2006**, *8*, 3137-3139.
(43) Eliel, E. L.; Wilen, S. H. *Stereochemistry of Organic Compounds*; John Wiley & Sons, New York, Chichester, Brisbane, Toronto, Singapore, 1994.
(44) Brutiu, B. R.; Iannelli, G.; Riomet, M.; Kaiser, D.; Maulide, N. Stereodivergent 1,3-difunctionalization of alkenes by charge relocation. *Nature* **2024**, *626*, 92-97.
(45) N, G. S.; Brutiu, B. R.; Kaiser, D.; Maulide, N. Cationic, Iodine(III)-Mediated and Directed Diastereoselective Oxidation of Inert C-H Bonds in Cyclic Hydrocarbons. *Angew. Chem. Int. Ed. Engl.* **2025**, e202421872.
(46) Bégué, J. P.; Bonnet-Delpon, D. Cyclic oxonium salts: 13C magnetic resonance spectroscopy. The correlation of chemical shifts with the calculated charge density. *Org. Magn. Res.* **1980**, *14*, 349-355.
(47) Lubinskaya, O. V.; Shashkov, A. S.; Chertkov, V. A.; Smit, W. A. Facile Synthesis of Cyclic Carboxonium Salts by Acylation of Alkenes1. *Synthesis* **1976**, 742-745.
(48) Wang, M. Enantioselective Intramolecular 1,5-Hydride Transfer/Cyclization through the Direct

586 Functionalization of C(sp3)-H Bonds Adjacent to a Heteroatom: From Nitrogen to Oxygen.
587 *ChemCatChem* **2013**, *5*, 1291-1293.
588 (49) Wang, L.; Xiao, J. Advancement in Cascade [1,n]-Hydrogen Transfer/Cyclization: A Method for
589 Direct Functionalization of Inactive C(sp^3)-H Bonds. *Adv. Synth. Catal.* **2014**, *356*, 1137-1171.
590 (50) Haibach, M. C.; Seidel, D. C-H bond functionalization through intramolecular hydride transfer.
591 *Angew. Chem., Int. Ed. Engl.* **2014**, *53*, 5010-5036.
592 (51) Peng, B.; Maulide, N. The redox-neutral approach to C-H functionalization. *Chem. Eur. J.* **2013**,
593 *19*, 13274-13287.
594 (52) Pan, S. C. Organocatalytic C-H activation reactions. *Beilstein. J. Org. Chem.* **2012**, *8*, 1374-1384.
595 (53) Wang, B.; Gandamana, D. A.; Gagosz, F.; Chiba, S. Diastereoselective Intramolecular Hydride
596 Transfer under Bronsted Acid Catalysis. *Org. Lett.* **2019**, *21*, 2298-2301.
597 (54) Simmons, E. M.; Hartwig, J. F. On the interpretation of deuterium kinetic isotope effects in C-H
598 bond functionalizations by transition-metal complexes. *Angew. Chem. Int. Ed. Engl.* **2012**, *51*, 3066-
599 3072.
600 (55) Overman, L. E.; Velthuisen, E. J. Scope and Facial Selectivity of the Prins-Pinacol Synthesis of
601 Attached Rings. *J. Org. Chem.* **2006**, *71*, 1581-1587.
602 (56) Overman, L. E.; Pennington, L. D. Strategic Use of Pinacol-Terminated Prins Cyclizations in
603 Target-Oriented Total Synthesis. *J. Org. Chem.* **2003**, *68*, 7143-7157.
604 (57) McCormack, A. C.; More O'Ferrall, R. A.; O'Donoghu, A. C.; Rao, S. N. Protonated Benzofuran,
605 Anthracene, Naphthalene, Benzene, Ethene, and Ethyne: Measurements and Estimates of pK_a and
606 pK_R. *J. Am. Chem. Soc.* **2002**, *124*, 8575-8583.
607